JOURNAL OF PROPULSION AND POWER
Vol. 18, No. 2, March–April 2002

Mach 8 Testing of a Scramjet Engine with Ramp Compression

Takeshi Kanda,* Kouichiro Tani,† Kan Kobayashi,‡ Toshihito Saito,§ and Tetsuji Sunami§
National Aerospace Laboratory, Miyagi 981-1525, Japan

To improve combustion efficiency and the inlet started condition, a scramjet model having a ramp combined with a single strut was tested under Mach 8 flight conditions at the Ramjet Engine Test Facility of the National Aerospace Laboratory, Japan. The attached ramp shielded some of the fuel injectors. The fuel flow rate from the open injectors to the flow path was designated as the effective fuel flow rate. In the tests, a combustion efficiency of 90% was attained with vertical injection of hydrogen fuel. The thrust increase was 590 N at the effective equivalence ratio of 1.3. However, because the engine geometry was not optimized, a sufficient increase of the thrust was not attained. High temperature and high pressure necessary for ignition and combustion were achieved by the ramp. When the pressure in the isolator was 160 times as high as that of the freestream air due to combustion, the inlet was in the started condition despite the high pressure. This improved started condition was attained by using the ramp to increase the pressure in the inlet.

Nomenclature

h	=	height of the backward-facing step, mm
P	=	pressure, Pa
w	=	engine width at the exit, mm
x	=	horizontal distance from the leading edge of the top wall, mm
$x1$	=	horizontal distance from the leading edge of the sidewall, mm
y	=	vertical distance from the top wall at the entrance position, mm
z	=	spanwise distance from the engine symmetry plane, mm
ΔF	=	thrust increase from that with no-fuel condition, N
ΔL	=	lift increase from that with no-fuel condition, N
ϕ	=	equivalence ratio

Subscripts

e	=	effective
t	=	total
w	=	wall
∞	=	freestream condition

Introduction

STUDIES of an aerospace plane are being carried out to create a new transportation system for use to and from a low Earth orbit. One of the engines being considered for use in this aerospace plane, the scramjet engine, is being studied at the National Aerospace Laboratory, Kakuda Research Center. In the Ramjet Engine Test Facility (RJTF) at the center, subscale scramjet research engine models have been tested under Mach 4, 6, and 8 flight conditions.[1] Detailed results of subscale scramjet engine tests other than those obtained in the RJTF[2–8] have not been open to the public, and thus the results of the RJTF have greatly contributed to the progress of scramjet engine research.

Received 19 December 2000; revision received 28 October 2001; accepted for publication 29 October 2001.

*Leader, Combined Cycle Engine System Group, Ramjet Propulsion Research Center, Kakuda. Senior Member AIAA.
†Senior Researcher, Ramjet Propulsion Research Center, Kakuda.
‡Researcher, Ramjet Propulsion Research Center, Kakuda. Member AIAA.
§Senior Researcher, Ramjet Propulsion Research Center, Kakuda. Member AIAA.

In the first series of the tests conducted under Mach 8 flight conditions, only a slight pressure increase by fueling was observed.[6] In this testing, the air was compressed only by sidewall contraction, and the pressure in the combustor was about 10 kPa. In the second series, an increase in pressure by combustion was attained by the addition of a strut, which resulted in a contraction ratio of 5 (Ref. 7). However, a large amount of fuel was necessary to attain this pressure increase. In the third series, a thicker strut was used, and a combustion efficiency of about 90% was attained.[8] However, the engine configuration with the thicker strut induced an unstarted condition for fuel flow rates above the stoichiometric one, and the combustion region was limited in the divergent section far downstream of the fuel injectors. The combustion induced a large Rayleigh heating total pressure loss. To improve the combustion conditions and startings, another modification of geometry was applied in the fourth series of the tests, specifically, ramp compression combined with the sidewall compression and the strut compression was introduced in the inlet.

As for the design of a combined-cycle engine with variable wall geometry, wedge-shaped sidewalls are not suitable for such variable geometry, and ramp compression achieved by a movable top wall is more promising. Thus, the present test results with the ramp are useful in understanding the characteristics of engines with ramp compression. The results of the testing, as well as discussion and analysis of the results, are presented in this paper.

Experimental Apparatus and Methods

Test Facility

The RJTF is equipped with a high-temperature, high-pressure air supply system and a vacuum ejection system. For these tests, the Mach number at the exit of the facility nozzle was 6.73. The total temperature and the total pressure of the air were 2600 K and 10.0 MPa, respectively. These correspond to flight conditions at Mach 8 with a flight dynamic pressure of 26 kPa. The relatively low dynamic pressure was due to the facility's capacity. Compressed air was heated by a ceramic storage heater and subsequently heated by a vitiation air heater. At the nominal operation, the flow rates of air, hydrogen, and oxygen for the vitiation heater were 6.16, 0.181, and 2.16 $kg \cdot s^{-1}$, respectively. The vitiated air contained 21% oxygen and 27% water in volume fraction. The supersonic facility nozzle had a square exit (51× 51 cm). The nominal static pressure at the exit of the nozzle, P_∞, was 1.6 kPa. The boundary-layer thickness was 90 mm at the engine entrance, according to pitot pressure measurements.[9] The inner surface of the top wall of the engine was level with that of the Mach 6.7 nozzle to ingest the boundary layer, simulating the entrance conditions of the engine attached to the surface of the aerospace plane.

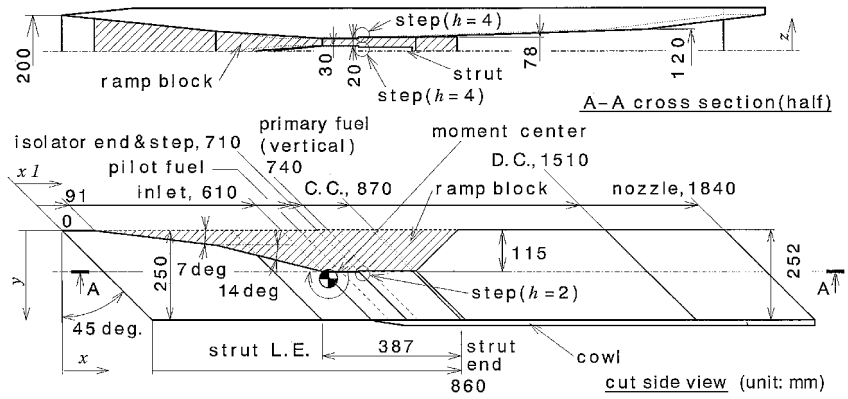

Fig. 1 Engine model.

Engine Model

Figure 1 shows a schematic diagram of the water-cooled engine model. The engine height was 250 mm. The top wall was at $y = 0$ mm, and the cowl inner surface was at $y = 250$ mm. The engine width was 200 mm, and the leading edges of the sidewalls were at $z = \pm 100$ mm. The swept angles of the sidewall and the strut were 45 deg, and the backward-facing step on the sidewall and the exit plane of the engine also had swept angles of 45 deg.

The hatched part is the ramp block, which was installed for the present tests. The overall contraction ratio of the engine is 9.3. The pressure at the exit of the facility nozzle is low in the RJTF, so that larger contraction attained by combination of the ramp and the sidewall was required to attain a sufficient pressure level in the combustor. The angles of the two-stage ramp surface were 7 and 14 deg from the horizontal line in the inlet. The first ramp started at $x = 91.4$ mm and the second ramp at $x = 445.6$ mm and $y = 45.4$ mm. The height of the ramp block was 115 mm at the end of the inlet. The parallel part of the ramp block continued to the end of the combustor. The angle of the rear face of the block was 45 deg.

Because it will be used for other tests at the RJTF in the future, the basic original engine model must be kept. If modification is necessary, however, some parts can be replaced with new ones, although replacable parts are limited. The original engine was designed by employing a combination of sidewall and strut compression. Therefore, a new top-wall plate was fabricated to attach the ramp block to the engine, and the ramp parts had to be located between the inlet and the combustor. The steep rear surface of the ramp block was unfavorable for production of thrust.

On the strut, as well as on the sidewall, the parallel geometry commenced at $x1 = 609.8$ mm. There was a backward-facing step at the junction of the isolator (Is.) and the combustor for 1) isolation of the pressure increase in the combustor and 2) flame holding. Its height was 4 mm on the sidewalls and on the strut and 2 mm on the top wall. The steps were located at $x1 = 709.8$ mm, 100 mm downstream of the inlet.

The model had no igniter. In previous testing, autoignition was attained under the Mach 8 flight conditions because of the high total temperature of the air.[8] The fuel, hydrogen, was injected vertically to the sidewalls through 12 holes, or parallel to the sidewalls through 14 holes on the steps. Their throat diameter was 1.5 mm. Fuel was injected at sonic conditions in the vertical injectors. The exit diameter of the parallel fuel injectors was 3.0 mm. The pilot fuel was supplied through 52 holes on the sidewalls upstream of the step under the sonic injection condition. The hole diameter was 0.5 mm. There were no fuel injection holes on the strut nor on the ramp block. The total temperature of the fuel was approximately 280 K, and the total pressure of the fuel varied according to the fuel flow rate.

These injection holes were open to the airflow. The engine model was originally designed with no ramp blocks. Therefore, the ramp blocks shielded 12 vertical injection holes, 10 parallel injection holes, and 42 pilot fuel holes on the sidewalls. These holes were not completely closed, and the same amount of the fuel leaked out from these shielded holes as under the no-ramp condition. The fuel flow conditions were confirmed by metering orifices and pressure in the fuel injection manifolds. The leaked fuel would not enter the combustor due to the high dynamic pressure of the airflow and was supposed to flow out to the rear of the ramp block. In the present paper, the flow rate of the fuel from the injectors open to the airflow is defined as the effective fuel flow rate, designated with the subscript e. The total fuel flow rate is the sum of the fuels from the open injectors and from the shielded injectors.

According to a three-dimensional viscous calculation on the previous engine configuration with a strut and no ramp block, the mass capture ratio was 0.85 (Ref. 10). The ramp configuration was designed so that the shock waves impinged on the cowl inner surface in the isolator, and the measured wall pressure in the inlet was maintained at the same level as that of the previous model, as will be discussed later. Therefore, the mass capture ratio of 0.85 was also adopted for the present engine in estimation of the equivalence ratio and for purposes of discussion. Thus, the fuel flow rate under the stoichiometric condition was 47 $g \cdot s^{-1}$.

Eighteen tests, 29–46, were planned. Of these, 13 tests were successful. Each test was divided in several stages, where a different kind of fuel supply condition was employed in each. These stages are designated with a single alphabet character. Together with the test number, a specific fuel supply stage is referred to, for example, as stage 37a, stage 37b, etc.

The engine wall was made of copper. The following engine components were individually cooled by water: 1) the leading edge of the inlet, 2) the inlet, 3) the top wall of the isolator/the constant duct part of the combustor, 4) the sidewalls of the isolator/the constant duct part of the combustor (C.C.) 5) the cowl, 6) the divergent duct part of the combustor (D.C.) 7) the nozzle, 8) the leading edge of the strut, and 9) the ramp block. The strut, except for its leading edge, was not cooled. The water passages for cooling were fabricated by machining and covered by electroforming, except for that of the strut and those of the ramp, which were fabricated by machining and brazing.

Measurements

Wall Pressure, Wall Temperature, and Heat Flux

Wall pressure and wall temperature at 1 mm from the inner surface of the model were measured. In the present paper, the wall pressure is nondimensionalized by the nominal static pressure at the exit of the facility nozzle. The top-wall pressure at $x1 = 1040$ mm of the ramp model was measured on the rear surface of the ramp. The measurement error of the nondimensionalized wall pressure was ± 0.06 in the nozzle and the inlet and ± 0.3 in the isolator and the combustor. Temperature of the coolant water was measured at the entrance manifold and at the exit for each engine component listed.

Forces and Moment

Thrust, lift, and pitching moment were measured by a floating frame force measurement system (FMS). The error for force

measurements was ±50 N. The center of pitching moment was set at $x = 741.43$ mm and $y = 135.8$ mm.

The drag, the lift, and the pitching moment in the no-fuel condition as measured by FMS were 980 N, 665 N, and 236 N · m, respectively. The forces measured by FMS contained drag, which should not be included in the net force estimation. The increases of the thrust and the lift caused by fueling from those in the no-fuel condition will be shown and discussed subsequently.

Gas Sampling

Gas sampling was carried out at 14 locations at the exit of the engine model using probes, each with a fine sampling orifice of 0.3 mm, after probe calibration.[11]

One-Dimensional Calculation

A one-dimensional calculation was conducted to estimate the kinetic energy efficiency of the inlet and the combustion efficiency. The supersonic nozzle flow from the plenum chamber was also simulated. The calculation procedure was as follows:

1) The temperature of the vitiated air and the flow rates of the air, hydrogen and oxygen to the vitiation heater were specified. The total pressure was calculated from the choking condition at the facility nozzle. The throat was square, 32.5 × 32.5 mm. The calculated total pressure agreed with the nominal value.

2) The exit size of the facility nozzle was corrected with the measured average displacement thickness of 25 mm (Ref. 9). The vitiated air was assumed to expand isentropically in the nozzle. The calculated Mach number and the static pressure at the nozzle exit agreed with the nominal values.

3) The effect of the swept angle of the engine was ignored, and the distance from the leading edge was used when the calculated results were compared with the experimental data.

4) The air and the combustion gas were assumed to be in the equilibrium condition throughout the engine.

5) The mass capture ratio was 0.85, according to the previous estimation by computational fluid dynamics (CFD).[10]

6) The specified part of the fuel reacted in a stoichiometric condition at the specified location. The ratio of the reacted fuel to the total fuel represented combustion efficiency here. The residual fuel mixed with the residual air. The combustion efficiency was estimated by comparison of the calculated pressure and the measured wall pressure.

7) The pressure on the rear surface of the ramp block in the combustor was calculated utilizing two-dimensional Prandtl–Meyer flow. The expanded flow condition behind the ramp block was calculated with the impulse function from the combustor and the estimated rear-surface pressure of the ramp.

8) The combustion gas expanded isentropically downstream of the ramp to the exit of the nozzle.

9) The boundary layer was turbulent throughout the engine. The friction coefficient was calculated using the formula of van Driest (see Ref. 12).

10) The inviscid flow condition and the inviscid thrust were calculated first. Next, the friction drags were subtracted from the inviscid thrust, and the net thrust was estimated.

Experimental Results

In this section, the measured forces and moment are presented first to clarify the characteristics of the engine operations. Then, the detailed results, that is, wall pressure distributions, etc., are presented.

Thrust, Lift, and Pitching Moment

Figures 2a–2c show the increments of the thrust and the lift and the pitching moment. They were measured by FMS. In the mV condition, fuel was injected vertically. When the sidewall pilot fuel injection was combined with the mV condition, the test results were included in the mV in Figs. 2, because the flow rate of the sidewall pilot injection was less than $\phi_e = 0.1$. In the sP + mV condition, the sidewall pilot fuel (sP) more than $\phi_e = 0.1$ and the vertically injected fuel more than $\phi_e = 1.0$ were injected. In the mP + (sP or mV) condition, the parallel injection (mP) was used with the pilot fuel injection or the vertical fuel injection.

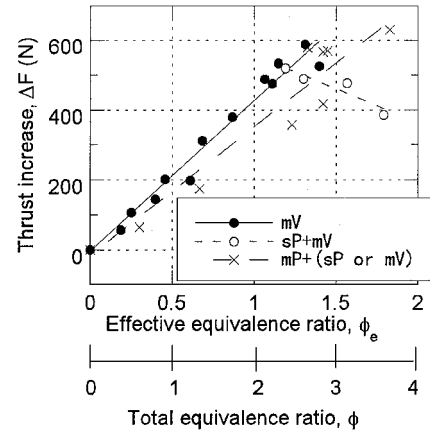

a) Thrust increase from no-fuel condition

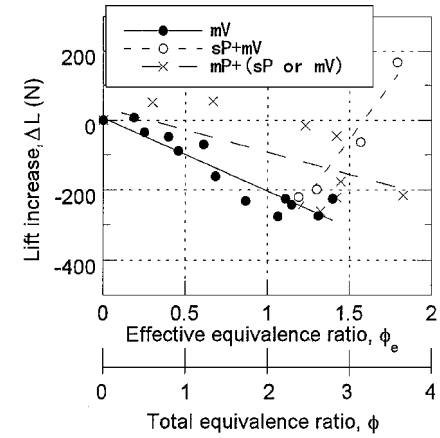

b) Lift increase from no-fuel condition

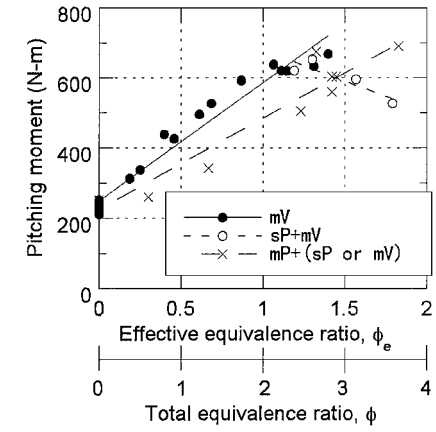

c) Pitching moment

Fig. 2 Forces and moment.

When the vertical fuel injection was used, the increase of thrust was proportional to the fuel flow rate, the same as for the lift and the moment. There were no abrupt changes due to the fuel flow rate, in contrast with the changes observed in the Mach 6 flight condition tests.[3,13] Proportionality was observed in the previous Mach 8 condition testing with the strut model.[8] The net drag in the no-fuel condition was estimated to be 660 N, according to the force measurement in the supplementary testing.[14] At $\phi_e = 1.3$ in the stage 39b test condition, the net thrust was estimated to be −70 N.

The momentum contribution to the thrust increase by the parallel fuel jet was estimated to be 110 N at $\phi_e = 1$. One-third of the thrust increase at the parallel-fueled condition was produced by this gas

jet. When the fuel flow rate from the pilot fuel injectors was large, the measured thrust decreased, and the lift increased. However, there was no unstarted condition in the wall pressure distribution, as will be shown.

Combustion with Vertical Fuel Injection

Wall Pressure Distribution

Figures 3a–3c show the wall pressure distributions with the vertical fuel injection from the sidewalls. The fuel flow rates and the thrusts are listed in Table 1. The pressure of the top wall was measured along the centerline of the channel. In the isolator and the constant duct part of the combustor, the wall pressure was obtained on the ramp block surface. On the top wall, the pressure level in the inlet was high due to the shock waves from the ramp even in the no-fuel condition. Around $x = 1300$ mm, the shock wave from the cowl impinged on the top wall.

At $y = 240/210$ mm, the pressure distribution in the inlet was the same as that of the strut model in the started condition.[7,8] It suggested that the airflow condition around the open bottom of the inlet was equivalent to that of the strut model previously tested, and thus, as mentioned in the earlier, the mass capture ratio of 0.85 of the previous engine model was also applicable to the present model.

As the fuel increased, the pressure increased in the isolator and the combustor. At $y = 125$ mm on the sidewall, the pressure did not increase in the isolator. In the stage 39b test, there was the maximum thrust increase without the parallel fuel injection. Even at the $\phi_e = 1.3$ vertical fuel injection condition of stage 39b, there was no pressure change in the inlet. This proves that the engine was in the started condition.

The one-dimensional simulation result is plotted in Fig. 3d with the test results of stage 37c. The fuel of $\phi_e = 1.1$ was injected vertically in the calculation and the experiment. In the calculation, the kinetic energy efficiency was 0.99, and the combustion efficiency was 0.9. The calculated result agreed well with the experimental results.

Equivalence Ratio and Combustion Efficiency

Figures 4 and 5 are the local equivalence ratios and the combustion efficiencies, respectively, measured at the exit of the engine. The

Table 1 Fuel flow rates and thrust increases at vertical fuel injection/sidewall pilot fuel injection

Test	Effective fuel flow rate, $g \cdot s^{-1}$		Effective equivalence ratio	Total fuel flow rate, $g \cdot s^{-1}$	Total Equivalence ratio	Thrust increase, N
	Vertical	Sidewall pilot				
36b	9	3	0.2	23	0.5	107
36d	29	3	0.7	64	1.4	311
37b	50	4	1.1	107	2.3	534
37c	50	0	1.1	100	2.1	488
39b	62	0	1.3	123	2.6	589
42c	63	3	1.4	131	2.8	526
38d	51	11	1.3	120	2.6	489
39d	62	23	1.8	164	3.5	386

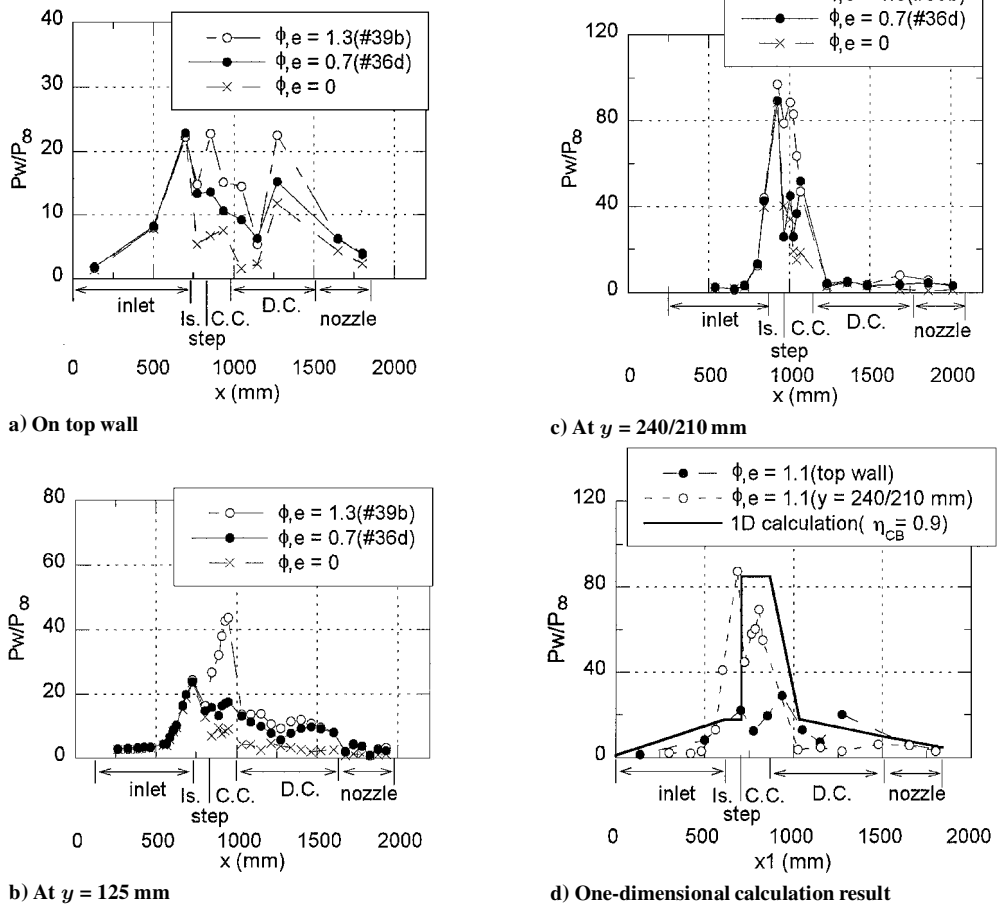

Fig. 3 Wall pressure distributions with vertical fuel injection.

Table 2 Fuel flow rates and thrust increases at parallel fuel injection/vertical fuel injection

Test	Effective fuel flow rate, $g \cdot s^{-1}$			Effective equivalence ratio	Total fuel flow rate, $g \cdot s^{-1}$	Total Equivalence ratio	Thrust increase, N
	Vertical	Parallel	Sidewall pilot				
40b	0	11	3	0.3	24	0.5	64
42b	0	64	3	1.4	115	2.4	417
41b	47	12	3	1.3	120	2.6	579
41d	29	36	3	1.4	125	2.7	569

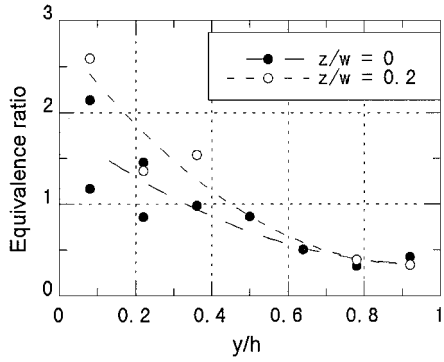

Fig. 4 Local equivalence ratios at the exit of the engine model with $\phi_{,e} = 1.1$ injected vertically.

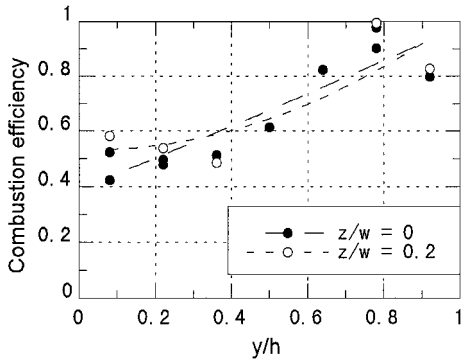

Fig. 5 Local combustion efficiency at the exit of the engine model with $\phi_{,e} = 1.1$ injected vertically.

fuel flow rate was $\phi_e = 1.1$ and was the same as that of stage 37b. Here, $z/w = 0$ is the symmetry plane, and $z/w = 0.5$ is the sidewall surface at the exit of the engine. The fuel hydrogen from the shielded injectors is injected with negligible momentum. Therefore, hydrogen concentration became high behind the ramp, that is, near the top wall. At the same time, because the air mass flux was larger around the cowl, the measured equivalence ratio became even lower near the cowl than near the top wall. The combustion efficiency was 0.8–1 near the cowl, whereas it was as low as 0.5 near the top wall.

The dynamic pressure of the airflow was high near the cowl and was estimated to be 500 kPa, which was calculated with the wall pressure and the assumption of isentropic change. The penetration of the fuel was estimated to be 3 mm with the empirical equation,[15] which was smaller than the width between the sidewall and the strut of 20 mm. This caused the low fuel concentration around the center plane.

Effect of the Sidewall Pilot Fuel Injection

Figures 6a and 6b show the effect of the sidewall pilot fuel injection. The total fuel flow rate of stage 38d was the same as that of stage 39b. The pilot fuel injectors were located in the isolator upstream of the backward-facing step. They were originally designed for flame holding at the step. When the pilot fuel injection was adopted, the pressure in the isolator was higher than that at the exit of the inlet and was 160 times as high as that of the freestream air. During the previous tests of the Mach 8 condition at the RJTF, the highest pressure was caused by the shock waves in the inlet, not by combustion or fuel injection.[8]

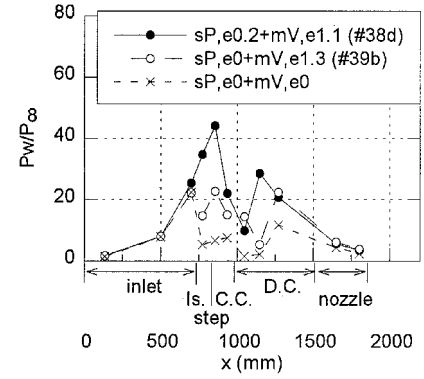

a) On top wall

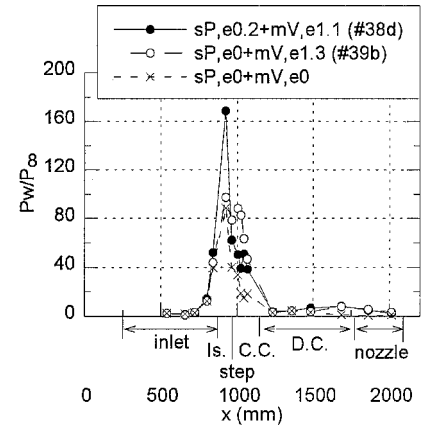

b) At $y = \frac{240}{210}$ mm

Fig. 6 Effect of sidewall pilot fuel injection on wall pressure.

Effect of the Parallel Fuel Injection

Table 2 details the effect of the parallel fuel injection in the form of a thrust increment. In the stage 41b and the stage 41d tests, the total fuel flow rates were comparable, but the ratio of the fuel flow rate by the parallel injection was different. The thrust was 10 N smaller in the stage 41d condition than in stage 41b. As was mentioned, the momentum thrust of the parallel injection was 110 N at $\phi_e = 1.0$, and so 24 $g \cdot s^{-1}$ ($\phi_e = 0.5$) should produce a 50-N increment in thrust. However, the difference of thrust between stages 41d and 41b was found to be quite small. This result implied that the momentum effect was virtually canceled by the weaker combustion pressure rise in stage 41d. This leads to the conclusion that the thrust increment due to the combustion by the parallel injection of the fuel was small.

Heat Flux

Two shock waves from the ramp corners impinged on the leading edge of the strut at different locations. The first shock was designed to impinge at $y = 150$ mm and the second one at the foot of the strut. The local intensive heat flux by the shock–shock interaction had been expected.[16] However, no notable local heat mark was observed on the strut surface. There was no mark on the leading edge of the cowl, either. The material of the strut and the cowl was copper, and the heat was conducted quickly.

In the no-fuel condition of the present model, the temperature of the coolant water of the strut leading edge increased by 4.2 K at the exit of the cooling channel at the cooling water flow rate of

0.25 kg · s^{-1}. In the previous strut model with no ramp, the temperature increased by 4.1 K at the flow rate of 0.24 kg · s^{-1} (Ref. 8). Because the exposed portion of the leading edge of the strut was smaller in the present model than in the previous model, the heat flux became larger and the total amount of the transferred heat was similar. This was caused by the ramp shock waves.

Discussion

Started Condition of Inlet

On the top wall, there was a thick boundary layer from the Mach 6.7 supersonic nozzle and the step height was lower than that on the sidewall. The influence of the pressure increase in the combustor propagated upstream of the step on the top wall. However, the engine model showed good startability. Because of the pressure increase resulting from combustion, a shock train was created in the isolator, which eventually reached the entrance of the isolator.

The length of the shock train was estimated by an empirical equation with the following assumptions.[17] The equation is for cylinder ducts, and so the hydraulic diameter at the isolator (width 20 mm × height 135 mm) was used in place of the duct diameter in the equation. The height of the low-speed region was greatest on the top wall, and the pressure increase due to combustion propagated first on the top wall. Thus, the properties of the boundary layer on the top wall were adopted in applying the equation.

Around the top wall in the no-fuel condition, the Mach number and velocity at the entrance of the isolator were estimated to be 5.4 and 2100 m · s^{-1}, respectively, from the wall pressure and the assumption of the isentropic change. The displacement thickness was used in place of the momentum thickness in the equation. The displacement thickness at the engine entrance was 33 mm. The displacement thickness in the isolator was estimated by using the ratio of the height of the engine to the displacement thickness, as follows.

When the capture ratio of 0.85 was multiplied by the engine height of 250 mm, the effective engine height at the entrance was 213 mm. The ratio of the displacement thickness of 33 mm to the height of 213 mm was 0.15 at the engine entrance. In the isolator, the displacement thickness was supposed to have a similar ratio to the engine height, and so the displacement thickness in the isolator was estimated to be 20 mm.

When the displacement thickness of 20 mm was used, the estimated lengths of the shock train on the top wall in the isolator were 39 and 180 mm for the ratios of the pressure increase of 3 and 5.5, respectively. The ratio of 3 was recorded at the vertical fuel injection test of stage 39b with $\phi_e = 1.3$. The estimated length 39 mm was shorter than the length of the isolator, that is, 100 mm. In the test of stage 39b, the pressure on the top wall of the isolator increased by combustion. However, that in the inlet did not, as shown in Fig. 3a. When the pilot fuel injection was used with the vertical fuel injection in stage 38d, the pressure ratio was 5.5, and the pressure on the top wall increased at the exit of the inlet. The estimated length of the shock train, that is, 180 mm, was about twice that of the isolator. However, the inlet was not in the unstarted condition in stage 38d.

The airflow conditions on the second ramp were also estimated from the wall pressure of 38 kPa: Mach number of 4.2 and velocity of 2000 m · s^{-1}. The shock train length was estimated again with these values as the entrance conditions of the shock train. The estimated shock train length was 15 mm for the same downstream pressure increase of stage 38d. The decrease of the pressure ratio suppressed the length of the shock train. In the experiments, the thickness of the boundary layer on the inlet ramp would be smaller than that at the entrance of the isolator due to the higher pressure. It could also shorten the influence length and suppress the unstarted condition.

Even when the pilot fuel was injected with the vertically injected fuel more than $\phi_e = 1$, the inlet was still in the started condition in spite of the large pressure increase in the isolator. However, the thrust decreased, and the lift increased as shown in Fig. 2. Spillage of the combustion gas over the leading edge of the cowl was observed from still photographs (not shown here). Thus, it can be assumed that the separation on the cowl was enlarged by the pilot fuel injection, and the separation reached the leading edge of the cowl. The spillage virtually increased the wedge angle and, thus, the pressure on the cowl outer surface. The increased pressure was presumed to induce the thrust decrease and the lift increase. At the same time, the pitching moment decreased because the leading edge of the cowl was located below and downstream of the moment center (Fig. 1). The decrease of the captured airflow also decreased the thrust.

Combustion in the Ramp Compression Model

Vertical Fuel Injection

Because the calculated wall pressure agreed reasonably well with those in the experiment, it is reasonable to assume that the kinetic energy efficiency of the inlet and the combustion efficiency for the effective fuel flow rate were actually the specified values of 0.99 and 0.9, respectively, in the experiments. Here, the reason for such high combustion efficiency is discussed.

By increasing the fuel flow rate, pressure in the isolator and the combustor increased first on the top wall, then on the $y = 125$ mm line, and finally near the cowl (Figs. 3a–3d). In the present model, the combustion was supposed to start around the top wall, then propagate toward the cowl.

Ignition requires high temperature.[18] It is attained in the low-speed region where the temperature is recovered. The displacement thickness of the boundary layer was estimated to be about 20 mm on the top wall of the isolator. In addition, a separation region was observed downstream of the ramp in a preliminary test.[19] This indicates the existence of a thick low-speed region on the top wall.

In the present engine, the vertical fuel injectors were located far downstream of the backward-facing step. When the injected fuel flow rate is small, the upstream-influence distance of the fuel jet is short, and the jet does not interact with the reattached primary flow downstream of the step. However, in the low-speed region, the dynamic pressure was small, and the penetration and the upstream-influence distance of the fuel increased. At the same time, the reattached point of the primary flow moves downstream as the low-speed region thickens.[20] In the low-speed region near the top wall, the fuel injected from the sidewall would interact with the primary flow. This interaction would create a large separation region downstream of the step. In this region, the recovery temperature is sufficiently high for ignition of hydrogen. As the fuel flow rate increased, the region of the interaction would spread upstream and toward the cowl.

The succeeding combustion requires high pressure.[18] In the combustion region, the pressure was 20–120 kPa, the average being 70 kPa. It was higher than the pressure predicted using simple models for combustion at half-atmosphere pressure.[21] The present engine configuration enabled sufficient recoveries of temperature and pressure, attaining the high combustion efficiency as shown in Fig. 5.

The results of the gas sampling conducted at the exit of the engine showed the existence of the low combustion efficiency around the top wall region. The gas from the combustor turns upward to the top wall due to the swept angle of the sidewall in the divergent section, as well as expands behind the ramp block. The nonreacted airflow around the center plane also flowed toward the top wall. The hydrogen from the shielded injectors would mix with the nonreacted air behind the ramp block, where the pressure and the temperature levels were low for combustion. As a result, the mixture would reduce the combustion efficiency measured at the exit of the engine.

Even though the high combustion efficiency was attained, the produced thrust was not sufficient. The low-thrust level was caused by the geometrical penalty of the rear angle of the ramp block. The pressure on the rear surface was low due to the quick expansion. According to the one-dimensional simulation, the net thrust will become 300 N with isentropic expansion in the divergent section.

Pilot Fuel Injection Upstream of the Step

When the vertically injected fuel flow rate was larger than unity, the pilot fuel injection increased the pressure in the isolator (Figs. 6a and 6b). The distance from the wall to the Mach disk and the length of the upstream influence of the pilot fuel jet were estimated by an

empirical equation.[15] The inflow condition of stage 37c was adopted, in which only the vertical injection with $\phi_e = 1.1$ was used. When the kinetic energy efficiency was 0.99, that is, the total pressure efficiency was 0.74, the Mach numbers became 3.2 around the cowl and 4.7 around the top wall, according to the measured wall pressure. The distances to the Mach disk were 0.5 mm around the cowl and 0.9 mm around the top wall with the effective equivalence ratio of the pilot fuel of 0.2, which corresponded to the fuel conditions of the stage 38d test. The upstream influence distances were 4 and 7 mm, respectively.

These small values were caused by the small diameter of the pilot fuel injector. There would be no intensive effect on the airflow by the pilot fuel jet with no combustion. The observed pressure increase with the pilot fuel injection was caused by the combustion of the pilot fuel injected into the low-speed region. If the pressure increase in the isolator had been caused by the separation shock due to the pilot fuel jet with no combustion, the effect would have appeared in any vertical-fuel-injection conditions. In the experiments, no pressure increase was observed with the pilot fuel injection in the isolator until the vertically injected fuel flow rate became about $\phi_e = 1$.

Heat Flux on the Leading Edge of the Strut

Because of the higher pressure caused by the ramp shock wave, the mean heat flux to the strut became larger than that in the strut model with no ramp. The heat flux on the leading edge of the strut was estimated by the method of Beckwith and Gallagher.[22] The inflow conditions were calculated using the shock wave relations. The nose radius of the leading edge of the strut was 1 mm.

The heat fluxes on the stagnation line of the leading edge were 16 $MW \cdot m^{-2}$ behind the first ramp shock wave and 22 $MW \cdot m^{-2}$ behind the second ramp shock wave. When both 30-mm strut surfaces from the leading edge, which were the sides of the cooling channel, were included in the heat flux estimation, the average fluxes around the cooling channel were 5.0 and 7.6 $MW \cdot m^{-2}$, respectively. The portion of the strut exposed to the airflow was 180 mm at the leading edge, 100 mm of which was downstream of the first ramp shock wave, 10 mm of the latter also being behind the second shock wave. The average heat fluxes around the channel were 4.2 $MW \cdot m^{-2}$ based on geometrical averaging. The heat transfer to the cooling water was 64 kW.

On the other hand, the heat flux on the stagnation line of the strut model with no ramp compression was 10 $MW \cdot m^{-2}$. The average heat flux around the channel was 2.9 $MW \cdot m^{-2}$ with no ramp shock effect, whereas the heat transfer to cooling water was 62 kW.

The obtained compatibility of the amount of heat agreed with the experimental value for in the increases of the coolant temperature at the exit manifold. The heat flux on the leading edge of the strut became about twice that when there was no ramp shock. As explained, the strut should be used to increase the low-pressure level of the incoming airflow in the present tests. However, generally, the strut should not be used with the ramp compression due to the higher heat flux.

Conclusions

A scramjet engine model with ramp compression was tested under the Mach 8 flight condition in the RJTF to improve the combustion performance and started condition of the inlet. The engine contraction ratio was 9.3. The following points were clarified:

1) A combustion efficiency of 80–90% was attained with the vertical fuel injection. The thrust increase was 590 N at the $\phi_e = 1.3$ condition. Because the ramp block was a temporary element and the engine geometry was not optimized, a sufficient increase of the thrust was not attained.

2) High temperature for ignition would be attained in the low-speed region in the combustor. High pressure for burning was attained by the compression of the ramp in the combustor. They contributed to the high combustion efficiency.

3) When the pressure in the isolator was 160 times as high as that of the freestream air due to combustion, the inlet was in the started condition despite the high pressure. This was caused by the high pressure on the ramp of the inlet.

Acknowledgments

The authors wish to thank the members of the scramjet research group of the National Aerospace Laboratory for cooperation in testing, data processing, and discussion.

References

[1] Yatsuyanagi, N., Chinzei, N., Mitani, T., Wakamatsu, Y., Masuya, G., Iwagami, S., Endo, M., and Hanus, G., "Ramjet Engine Test Facility (RJTF) in NAL–KRC, Japan," AIAA Paper 98-1511, April 1998.

[2] Sunami, T., Sakuranaka, N., Tani, K., Hiraiwa, T., and Shimura, T., "Mach 4 Tests of a Scramjet Engine: Effect of Isolator," *Proceedings of 13th International Symposium on Airbreathing Engines*, AIAA, Reston, VA, 1997, pp. 615–625.

[3] Kanda, T., Hiraiwa, T., Mitani, T., Tomioka, S., and Chinzei, N., "Mach 6 Testing of a Scramjet Engine Model," *Journal of Propulsion and Power*, Vol. 13, No. 4, 1997, pp. 543–551.

[4] Mitani, T., Hiraiwa, T., Sato, S., Tomioka, S., Kanda, T., and Tani, K., "Comparison of Scramjet Engine Performance in Mach 6 Vitiated and Storage-Heated Air," *Journal of Propulsion and Power*, Vol. 13, No. 5, 1997, pp. 635–642.

[5] Wakamatsu, Y., Chinzei, N., Ono, F., Saito, T., Kanda, T., Tomioka, S., and Yatsuyanagi, N., "Design and Preliminary Experiments of Liquid Hydrogen Cooled Scramjet Engine," *Proceedings of the 12th International Symposium on Space Technology and Science*, Japan Society for Aeronautical and Space Sciences, Paper 98-a-1-27, May 1998.

[6] Saito, T., Wakamatsu, Y., Mitani, T., Chinzei, N., Shimura, T., and Kanda, T., "Mach 8 Testing of a Scramjet Engine Model," *Proceedings of the 20th International Symposium on Space Technology and Science*, Vol. 1, Japan Society for Aeronautical and Space Sciences, Tokyo, 1996, pp. 58–63.

[7] Tomioka, S., Kanda, T., Tani, K., Mitani, T., Shimura, T., and Chinzei, N., "Testing of a Scramjet Engine with a Strut at Mach 8 Flight Condition," AIAA Paper 98-3134, July 1998.

[8] Kanda, T., Sunami, T., Tomioka, S., Tani, K., and Mitani, T., "Mach 8 Testing of a Scramjet Engine Model," *Journal of Propulsion and Power*, Vol. 17, No. 1, 2001, pp. 132–138.

[9] Hiraiwa, T., Mitani, T., Izumikawa, M., and Ono, F., "Calibration Studies of Nozzle Flow in Ramjet Engine Test Facility," *Proceedings of the 20th International Symposium on Space Technology and Science*, Japan Society for Aeronautical and Space Sciences, Paper 96-d-14, May 1996.

[10] Kodera, M., Sunami, T., and Nakahashi, K., "Numerical Analysis of Scramjet Combusting Flows by Unstructured Grid Method," AIAA Paper 2000-0886, Jan. 2000.

[11] Mitani, T., Takahashi, M., Tomioka, S., Hiraiwa, T., and Tani, K., "Analyses and Application of Gas Sampling to Scramjet Engine Testing," *Journal of Propulsion and Power*, Vol. 15, No. 4, 1999, pp. 572–577.

[12] White, F. M., *Viscous Fluid Flow*, McGraw–Hill, New York, 1974, pp. 632–640.

[13] Sato, S., Izumikawa, M., Tomioka, S., and Mitani, T., "Scramjet Engine Test at Mach 6 Flight Condition," AIAA Paper 97-3021, July 1997.

[14] Mitani, T., Kanda, T., Hiraiwa, T., Igarashi, Y., and Nakahashi, K., "Drag in Scramjet Engine Testing: Experimental and Computational Fluid Dynamic Studies," *Journal of Propulsion and Power*, Vol. 15, No. 4, 1999, pp. 578–583.

[15] Cohen, L. S., Coulter, L. J., and Egan, W. J., Jr., "Penetration and Mixing of Multiple Gas Jets Subjected to a Crossflow," *AIAA Journal*, Vol. 9, No. 4, 1971, pp. 718–724.

[16] Bertin, J. J., *Hypersonic Aerothermodynamics*, AIAA Education Series, AIAA, Washington, DC, 1994, pp. 537–555.

[17] Waltrup, P. J., and Billig, F. S., "Structure of Shock Waves in Cylindrical Ducts," *AIAA Journal*, Vol. 11, No. 10, 1973, pp. 1404–1408.

[18] Mitani, T., Chinzei, N., and Kanda, T., "Reaction- and Mixing-Controlled Combustion in Scramjet Engines," *Journal of Propulsion and Power*, Vol. 17, No. 2, 2001, pp. 308–314.

[19] Tani, K., Kanda, T., Kudo, K., and Akihisa, D., "Effect of Side-Spillage from Airframe on Scramjet Engine Performance," *Journal of Propulsion and Power*, Vol. 17, No. 1, 2001, pp. 139–145.

[20] Karashima, K., and Hasegawa, K., "An Approximate Approach to Base Flow Behind Two-Dimensional Rearward-Facing Steps Placed in a Uniform Supersonic Stream," Inst. of Space and Aeronautical Science, ISAS Rept. 501, Tokyo, Japan, 1973, pp. 375–384.

[21] Heiser, W. H., Pratt, D. T., Daley, D. H., and Mehta, U. B., *Hypersonic Airbreathing Propulsion*, AIAA Education Series, AIAA, Washington, DC, 1994, p. 233.

[22] Beckwith, I. E., and Gallagher, J. J., "Local Heat Transfer and Recovery Temperature on a Yawed Cylinder at a Mach Number of 4.15 and High Reynolds Numbers," NASA TR R-104, 1958.